Hybrid Nanosheets of an Inorganic–Organic Framework Material: Facile Synthesis, Structure, and Elastic Properties

Jin-Chong Tan, Paul J. Saines, Erica G. Bithell, and Anthony K. Cheetham*

Department of Materials Science and Metallurgy, University of Cambridge, Pembroke Street, Cambridge CB2 3QZ, U.K.

ABSTRACT

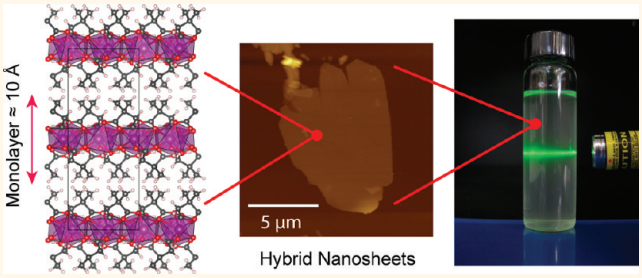

We report a new 2-D inorganic–organic framework material, MnDMS [Mn 2,2-dimethylsuccinate], featuring weakly bound hybrid layers in its bulk crystals that can be readily exfoliated into nanosheets *via* ultrasonication. The fully exfoliated hybrid nanosheets correspond to a unilamellar thickness of about 1 nm, while the partially exfoliated nanosheets (multilayer films) exhibit a typical thickness on the order of 10 nm. We used atomic force microscopy to characterize their surface topography and to map the variation of nanomechanical properties across the surface of the delaminated nanosheets. The morphology and crystallographic orientation of the exfoliated layers were further studied by transmission electron microscopy. Additionally, we investigated the elastic anisotropy underlying the bulk host material by means of single-crystal nanoindentation, from which the critical resolved shear stress (τ_{crit}) needed for the micromechanical delamination of individual layers was determined to be relatively small ($\lesssim$0.4 GPa).

KEYWORDS: inorganic–organic hybrid framework · metal–organic framework · nanosheet · thin films · exfoliation · mechanical properties · elastic anisotropy

Hybrid framework materials are crystalline compounds comprising inorganic and organic structural components coexisting as integral parts of an infinite network; their structures range from 1-D chains to 2-D layers and 3-D frameworks.[1] It is important not to confuse this new class of materials with hybrid nanocomposites,[2] whose inorganic and organic components exist as distinct and separate phases. There are two broad categories of hybrid framework materials: (i) dense hybrid frameworks, which often incorporate inorganic M–O–M (metal–oxygen–metal) arrays that provide the topological characteristics central to certain types of physical properties, such as ferromagnetism, photoluminescence, and electronic conductivity;[3,4] (ii) metal–organic frameworks (MOFs), which are nanoporous hybrid frameworks aimed at gas separations and storage,[5–7] catalysis,[8] drug delivery,[9] and sensing applications.[10]

Over the past decade, the field of hybrid framework materials has seen tremendous growth, and it is now relatively straightforward to synthesize systems of various chemistries and structures.[1,3] The hybrid framework compounds obtained, however, are largely micrometer-sized single crystals or polycrystalline powders, which are difficult to prepare as thin-film structures desirable for technological applications.[11,12] As such, recent activities have focused on the development of a variety of "bottom-up" methods for fabricating MOF thin films[11] and membranes.[13] Work concerned with application of a facile "top-down" approach, such as liquid exfoliation,[14,15] for producing crystalline films and nanosheets of hybrid framework materials still remains at the absolute minimum. In fact, only two studies[16,17] exist in the literature, both of which relate to layered MOF materials that can be delaminated into nanosheets *via* ultrasonication. Hitherto, the exfoliation of a dense hybrid framework material comprising M–O–M arrays has not been demonstrated. This is indeed surprising because, following the pioneering work in the 1990s,[15,18,19] the top-down exfoliation approach has been successfully adopted for preparing nanosheets covering a diverse range of layered materials, including metal

* Address correspondence to akc30@cam.ac.uk.

Received for review October 21, 2011 and accepted November 27, 2011.

Published online November 27, 2011
10.1021/nn204054k

oxides, metal hydroxides, perovskite-type structures, graphite, and so on.[14,20] Moreover, it is extremely promising to see that nanosheets produced as such can serve as precursors for creating continuous thin films[21,22] or can be further integrated with other matrices (*e.g.*, polymers) to form robust composite materials.[23]

In the present work, we demonstrate the exfoliation of a new hybrid framework material, Mn 2,2-dimethylsuccinate (MnDMS), which is dense and features 2-D layers that are held together by weak van der Waals interactions. The resulting 2-D material represents the first example of *single-phase* hybrid nanosheets prepared from a nonporous inorganic–organic framework *via* a "top-down" approach. The unique structure, morphology, and nanomechanical characteristics of MnDMS nanosheets are described below.

RESULTS AND DISCUSSION

1. Crystal Structure of Layered MnDMS Hybrid Framework. MnDMS, Mn 2,2-dimethylsuccinate [$Mn(C_6H_8O_4)(H_2O)$], crystallizes with an orthorhombic crystal structure (Figure 1a), in which 2-D hybrid layers are oriented perpendicular to the *c*-axis. Each layer is constructed from inorganic and organic building blocks that are covalently bonded together (Figure 1b) and features distorted MnO_6 octahedra. These octahedra form corner-sharing chains along the *b*-axis with 1-D inorganic (Mn–O–Mn) connectivity, and the chains are connected *via* bridging 2,2-dimethylsuccinate ligands to form the 2-D layers. The methyl groups of the ligand protrude out from these layers, providing them with hydrophobic caps on both sides (Figure 1a). Notably, these layers have a thickness of approximately 10 Å and interact with each other only *via* van der Waals interactions. The weak nature of these interactions is critical to the layers being readily separated using simple organic solvents.

The Mn cations are divalent and are crystallographically identical. They are coordinated to one oxygen atom from a water molecule and five oxygen atoms from four different carboxylate groups. The one carboxylate group whose oxygen atoms bond to the same Mn also has one oxygen, O4 (see Figure 1b), which is bonded to two different Mn cations, providing the corner-sharing chain connectivity. One of the Mn–O4 bonds is 2.457(2) Å, which is longer than any of the other Mn–O contacts, which lie between 2.110(2) and 2.181(2) Å. This suggests that the strength of the bonding in the chain direction (along the *b*-axis) is unlikely to be significantly stronger than in any of the other directions within a layer, despite the inorganic connectivity.

2. Exfoliation of Layered MnDMS into Hybrid Nanosheets. The liquid exfoliation procedure for MnDMS is straightforward, low cost, and high throughput. The bulk crystals were ultrasonicated in ethanol for a period of 20 min

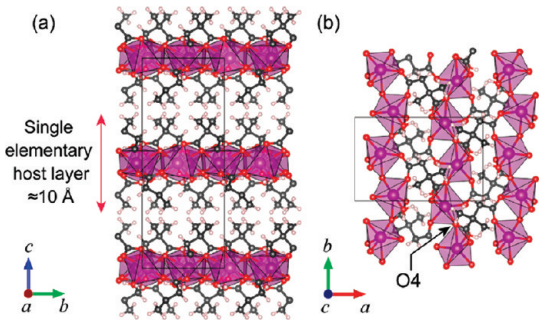

Figure 1. Crystal structure of $Mn(C_6H_8O_4)(H_2O)$ layered hybrid framework. (a) The arrangement of 2-D layers oriented parallel to the {001} planes, featuring methyl functional groups protruding into the interlayer space. (b) Structure of a single elementary host layer featuring the 1-D chains of distorted MnO_6 octahedra oriented along the *b*-axis. A close-up showing the coordination environment around the Mn center appearing in Figure S3 in the SI. The black outline denotes the orthorhombic unit cell. Magenta: manganese, red: oxygen, gray: carbon, white: hydrogen.

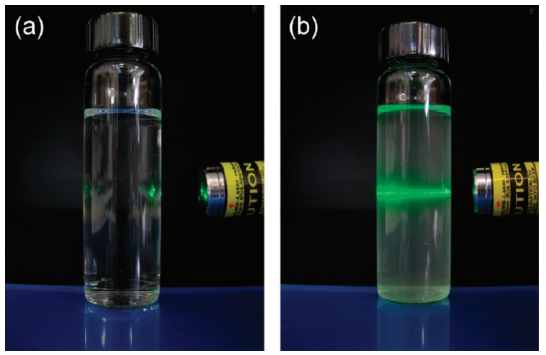

Figure 2. Demonstration of the Tyndall effect. (a) The path of the green laser beam is invisible in pure ethanol (ignoring reflections by the glass surfaces). (b) The laser beam is clearly visible through a colloidal solution comprising MnDMS nanosheets suspended in ethanol.

to obtain a milky colloidal suspension (0.14 mg/mL) comprising a mixture of fully exfoliated and partially exfoliated nanosheets. We have confirmed that such a colloidal solution exhibits the Tyndall effect (Figure 2), whereby the finely dispersed nanosheets in solution are capable of scattering an incident laser light beam. It is noted that a higher degree of exfoliation can be obtained by extending the sonication time. Apart from ethanol, we have also tried other solvents as the exfoliation agent, including water, methanol, propanol, hexane, and tetrahydrofuran (THF). Ethanol, however, was found to be the most efficient for exfoliating the layers and in preventing the isolated films from subsequent reassembly.

The nanosheets suspended in the colloidal solution were collected and dispersed onto a flat substrate for characterization under the atomic force microscope (AFM). As shown in Figure 3a, the fully exfoliated nanosheets display lateral dimensions of up to several

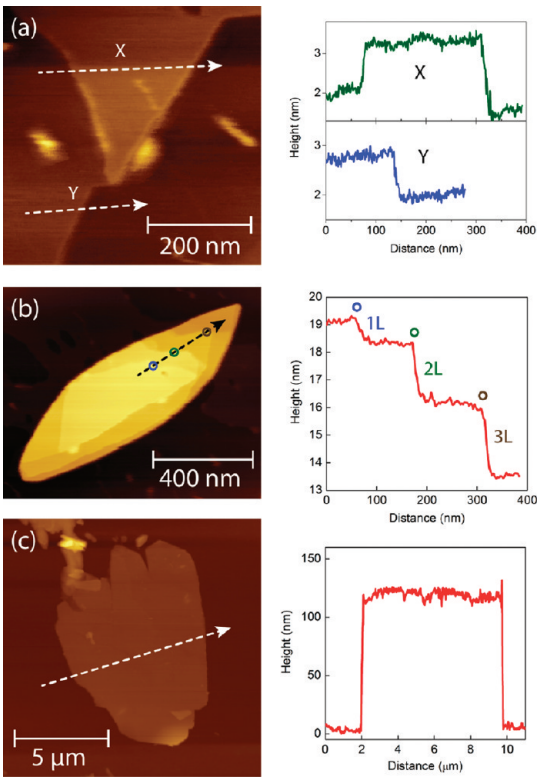

Figure 3. Surface topography of ethanol-exfoliated nanosheets acquired by AFM. (a) Two fully exfoliated unilamellar nanosheets, each featuring a single elementary host layer of *ca.* 1 nm thickness. (b) Partially exfoliated nanosheet, in which one, two, and three host layers (L) are discernible. (c) Multilayer film comprising about 100 host layers and with a relatively large lateral dimension of *ca.* 8 × 11 μm^2.

hundred nanometers across and feature a thickness of approximately 1 nm, which indeed corresponds to the thickness of one elementary host layer (Figure 1a). On the other hand, partially exfoliated nanosheets (Figure 3b and c) consist of multilayer films, with a typical thickness ranging from about 10 to 100 nm; their lateral dimensions can reach about 10 μm. We note that the lateral size of the unilamellar nanosheets is relatively small, probably because vigorous agitation *via* ultrasonication has led to the fragmentation of fragile 2-D layers. Instead, gentler agitation procedures reported for the exfoliation of inorganic nanosheets (*e.g.*, *via* intermittent shaking)[24] might be applicable here to yield larger lateral dimensions, if sought.

3. Characterization of Nanosheets by Transmission Electron Microscopy. Nanosheets exfoliated using two different solvents (ethanol and hexane) were examined by transmission electron microscopy (TEM). In both cases, samples suitable for microscopy were prepared by dropping 4 to 6 drops of the as-prepared suspension onto a holey amorphous carbon film supported on a standard 3 mm copper grid. No additional dispersal of the material was required or performed (*e.g.*, additional sonication).

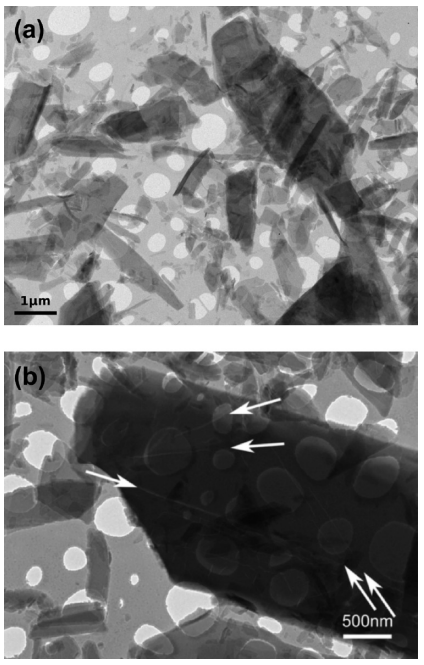

Figure 4. TEM bright-field images of ethanol-exfoliated nanosheets supported on a holey amorphous carbon film. (a) Typical morphology. (b) Larger multilayer film highlighting pre-exfoliation cracking along directions indicated by the arrows.

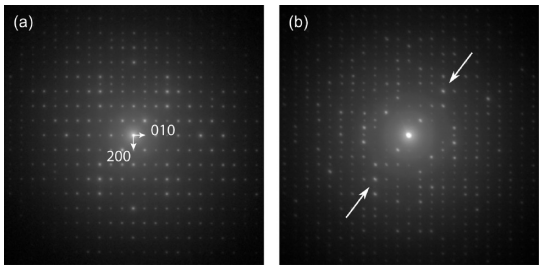

Figure 5. Selected area electron diffraction patterns from ethanol-exfoliated nanosheets. (a) From a larger, thicker nanosheet, showing a strong [001] crystallographic orientation, in which the reciprocal vectors are also indicated. (b) From a smaller, thinner nanosheet. Note the relatively stronger reflections along the arrowed direction and that the pattern is symmetrical on either side of this line. This is indicative of curling of the sheet in the (001) plane, rather than a simple tilt misorientation; the latter would cause greater asymmetry in the intensities of the reflections.

A bright-field image representative of the ethanol-exfoliated sample is shown in Figure 4a and confirms the predominant morphology. The exfoliated layers are generally longer than they are wide, with an aspect ratio of approximately 5:1. While the largest multilayer films observed under the TEM are as much as 5 μm in lateral dimension, there are numerous smaller sheets that are 100 nm in length, or less, consistent with AFM results (Figure 3). There is a clear, if qualitative, correlation between the size of a nanosheet and its thickness; the larger sheets are darker (and therefore thicker), and all sheets of the same size have similar transmitted

intensities. The only significant difference between the ethanol-exfoliated and hexane-exfoliated samples is that fragments of the former generally have sharper corners, whereas hexane exfoliation causes some rounding of the corner profiles (see Figure S5 in the Supporting Information (SI)).

Diffraction patterns obtained from such nanosheets demonstrate that, in all cases, the [001] zone axis is normal to the sheets (Figure 5a). High-quality, highly symmetric [001] zone axis patterns were obtained only from the thicker multilayered films. Interestingly, we discover that the best oriented diffraction patterns from the somewhat smaller (and therefore thinner) nanosheets indicate strong evidence for curling (Figure 5b), which tends to cause slight misorientation of the observed patterns from the exact [001] axis.

Given the relatively uniform morphology, aspect ratio, and orientation for the exfoliated nanosheets, one might expect to find common directions for the fragmented sheet edges. In fact, this is not the case. Images of many such fragments were correctly aligned with their corresponding diffraction patterns, but showed no evidence for common alignment of either the edges or the long axes of the fragments. Closer examination of the bright field images suggests a possible reason for this. As shown in Figure 4b, the surface of the thicker multilayer sheet features numerous cracks that are evidently a precursor to full exfoliation; while the symmetry of these cracks demonstrates that there are preferred crystallographic cleavage planes, it is equally clear that there are a number of "families" of crack orientations. We anticipate that there are several sets of cleavage planes that are rather similar in energy but crystallographically distinct. This will inevitably lead to the observed variety of orientations for the edges of the thinner exfoliated nanosheets.

4. Nanomechanical Property Mapping of Exfoliated Nanosheets. The nanomechanical characteristics of the nanosheets were measured under the atomic force microscope through implementation of the peak-force tapping mode.[25,26] Here we acquired the variation of the AFM tip force and the corresponding vertical displacement as it tapped across the surface of the nanosheet, from which the Young's modulus (E) property map (Figure 6a) can be constructed by analyzing the individual load−displacement (P−h) curves.

Figure 6 shows the results obtained from a multilayer nanosheet film comprising about 50 elementary host layers. It can be seen that the maximum vertical displacement (h) of the AFM tip remains below 2.5 nm (Figure 6b), indicating that material deformation is limited only to the first few elementary layers. Such vertical displacements gave rise to reaction forces of below 20 nN, as measured by the cantilever tip. The Young's modulus map (Figure 6a) shows that the elastic property of the

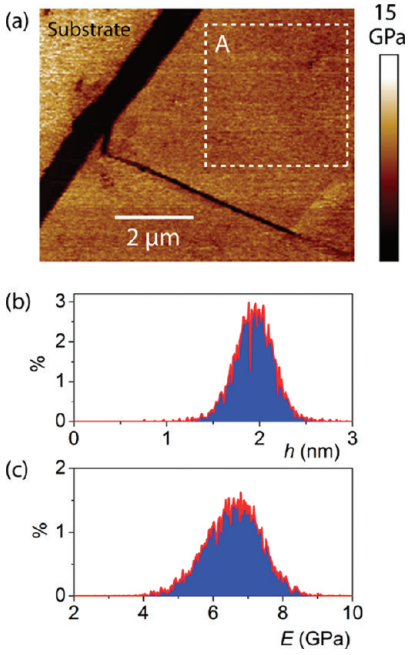

Figure 6. AFM nanomechanical property mapping of two MnDMS nanosheets located on a glass substrate (*NB*: the AFM tip used here is designed to measure $E \lesssim 20$ GPa). The thickness of nanosheet "A" is ~50 nm. The histograms correspond to data collected from the designated square. (a) Young's modulus map. (b) Vertical displacement (deformation) of the tip. (c) Histogram of Young's modulus.

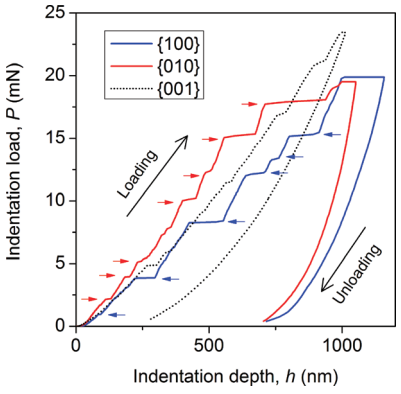

Figure 7. Typical nanoindentation load−displacement (P−h) curves on single crystals of MnDMS along the three principal directions of the orthorhombic crystal. The "pop-in" phenomena are displacement bursts (at a constant load) indicated by the horizontal arrows; these are more pronounced for the {100}- and {010}-oriented facets. Note that the {001} facet exhibits an appreciably larger elastic recovery upon unloading. The average values of the Young's moduli (E) were determined from surface penetration depths of 0 to 950 nm.

exfoliated nanosheet is largely homogeneous across the {001}-oriented surface; the histogram of the modulus map (Figure 6c) indicates that E is 6−7 GPa. Such a low elastic modulus resembles the stiffness property of organic polymers (0.1−21 GPa)[27] and MOFs (3−9 GPa),[28] whereas the elastic moduli of dense hybrid framework materials reported to date are typically above 10 GPa.[29]

5. Single-Crystal Nanoindentation Studies to Probe Elastic Anisotropy. To elucidate the structure−mechanical property relationships underlying the layered hybrid framework, we performed nanoindentation experiments on bulk crystals of MnDMS. A spherical-tip diamond indenter (10 μm radius) was employed so that the strain field induced under the tip is less localized, which is important for delaying the onset of irreversible deformation (plasticity). The {001}-, {010}-, and {100}-oriented crystal facets were indented (*i.e.*, along the three principal axes of the orthorhombic unit cell; see Figure 1), and a maximum penetration depth of 1000 nm was chosen in order to strain at least 1000 elementary host layers.

The load−displacement ($P-h$) curves obtained are presented in Figure 7. The nanoindentation results show that the average Young's moduli of the {001}-, {010}-, and {100}-oriented facets are (in GPa) 9.4 ± 0.3, 20.9 ± 0.2, and 13.6 ± 0.2, respectively. From these values, we established the ratios of the elastic moduli for the three orthogonal directions to be $E\{001\}$:$E\{010\}$:$E\{100\}$ = 1.00:2.22:1.45, demonstrating a marked change in stiffness exceeding 120%. Thus, it is clear that the layered MnDMS framework structure is highly anisotropic in nature. We see that the stiffest direction lies along the *b*-axis, which indeed corresponds to the orientation of the 1-D inorganic chains (Mn−O−Mn); cross-linking of the adjacent chains by the organic linkers is thought to have also contributed toward the relatively high elastic modulus observed here. In comparison, an intermediate modulus was measured along the *a*-axis, normal to the inorganic chains, suggesting that the bulky succinate ligands are relatively compliant building blocks, such that the anisotropy in the in-plane (2-D) direction can vary by more than 50%.

Given that the exfoliated nanosheets maintain the crystalline architecture of the parent material (Figures S2 in SI), it is reasonable to expect their in-plane elastic response to be reminiscent of the host structure (especially for multilayered films). On the other hand, the picture should be very different along the *c*-axis, for which the loading direction is perpendicular to the 2-D layers. We found that the elastic modulus determined from the bulk crystal along *c* gave the lowest modulus of all, $E\{001\}$ = 9−10 GPa (response of >1000 host layers); this is consistent with the view that adjacent layers held together by weak van der Waals forces can be more readily compressed together. In contrast, it is interesting to note that the corresponding modulus determined from the exfoliated nanosheet (*via* AFM; see Figure 6c) gave a value about 30% lower, as determined from the deformation of only a few host layers (Figure 6b). Our results therefore suggest that the stiffness property in the out-of-plane direction is size-dependent and that the compliance (*i.e.*, the inverse of stiffness, *E*) of the multilayered structure rises as the number of weakly bonded constituting host layers decreases.

We see that the $P-h$ curves of the {010} and {100} facets display significant "pop-in" phenomena (Figure 7), which are attributed to the shear-induced delamination of the weakly bonded layers. On the basis of knowledge of the critical load (P^*) corresponding to the first pop-in event, we applied the Hertzian elastic contact theory[30,31] to estimate the critical resolved shear stress (τ_{crit}) needed to initiate splitting of two adjacent layers. Our analysis (see SI for details) yielded relatively small τ_{crit} values of only 0.39 and 0.24 GPa, for shear stresses acting antiparallel to the [010] and [100] directions, respectively. An interesting comparison can be drawn against another dense layered hybrid framework material (copper phosphonoacetate, polymorph 2),[32] whose 2-D layers are hydrogen-bonded to each other and exhibit a τ_{crit} of approximately 1 GPa. Hydrogen bonds are typically an order of magnitude stronger than van der Waals interactions, which explains why the magnitudes of τ_{crit} estimated here for MnDMS are noticeably lower. Thus, our analysis confirmed that nanosheets can be more readily delaminated from systems with only van der Waals interactions between their layers. We envisage that micromechanical exfoliation may serve as a viable route to achieve hybrid nanosheets and thin-film structures (Figure S6 in the SI), especially when a better control of sheet thickness is sought.

CONCLUDING REMARKS

While this study focused only on the nanosheets of MnDMS, we have also discovered that it is possible to make similar layered hybrid framework structures with 2,2-dimethylsuccinic acid in combination with other transition metals, such as Co^{2+} and Zn^{2+} and that these, too, can be straightforwardly exfoliated by means of ultrasonication. In addition, we have found that similar hybrid structures can be obtained with monovalent cations, such as Li^{+}, and the much larger trivalent lanthanides, including La^{3+} and Y^{3+} (full details will appear in future publications). This shows that the bulky nature of the organic ligand is primarily responsible for the formation of 2-D layered hybrid frameworks, rather than the behavior of any particular cation. The thickness and the structure of the layer, in particular the cation coordination environments and the extent of inorganic connectivity, vary significantly between the different layered structures. In light of this, we anticipate that it should be possible to prepare hybrid nanosheets with distinctly different physicochemical properties by adopting the same synthetic route and exfoliation strategy presented here.

Finally, unlike porous MOFs, whose framework stability is often closely linked to the presence of solvents

trapped inside their cavities (*e.g.*, the removal of DMF molecules from MOF-2[16] appears to have caused some framework deterioration), the exfoliation of dense hybrid frameworks should be more straightforward in this respect given that their nonporous structures are inherently more robust.[29]

EXPERIMENTAL SECTION

Material Synthesis. Bulk crystals of MnDMS, $[Mn(C_6H_8O_4)(H_2O)]$, were synthesized hydrothermally using commercially available starting materials, which were utilized without further purification. A typical synthesis involved adding 55 mmol of $MnCl\cdot 6H_2O$, 84 mmol of 2,2-dimethylsuccinic acid, and 140 mmol of KOH to 9 mL of water (*i.e.*, corresponding to a mixture of 1:1.5:2.5:200). This mixture was placed in a 23 mL Teflon-lined Parr autoclave and heated at 140 °C for 3 days, after which the resulting product was filtered off and washed with water. After drying for an hour at 60 °C, inspection of the product showed that it contained colorless rod-shaped crystals suitable for single-crystal X-ray diffraction and nanoindentation studies. Phase purity was confirmed from powder X-ray diffraction patterns (see Figure S1 in the SI) collected on a Bruker D8 Advance diffractometer, using a linear position detector and Cu Kα radiation. The purity of bulk MnDMS was confirmed by microanalysis, which indicated that MnDMS contained 33.24% C and 4.61% H (calcd 33.20% and 4.64%, respectively).

Single-Crystal X-ray Diffraction. Single-crystal X-ray diffraction data for MnDMS were obtained at 120 K using an Oxford Diffraction Gemini Ultra diffractometer using Mo Kα radiation. This instrument was equipped with an Eos CCD detector, and the crystal was mounted on a cryoloop. Absorption corrections were carried out for these samples using analytical methods implemented in CrysAlisPro.[33] The structure was solved by using direct methods and subsequently refined against $|F|^2$ using SHELX-97[34] *via* the Win-GX interface (see Table S1 in the SI for summary of crystal data).[35] The displacement parameters of all non-hydrogen atoms were refined anisotropically, and the positions of the hydrogen atoms attached to the dicarboxylate ligands were geometrically constrained using the AFIX commands in SHELX-97. The aquo hydrogen atoms were readily located from the Fourier difference map. These were restrained to have a bond distance of 0.85 Å to the oxygen atoms to which they are attached, and the intramolecular bond angles of the water molecules were appropriately restrained. The thermal parameters of the methylene hydrogen atoms were constrained to be 1.2 times the carbon to which they are bonded, while the methyl hydrogen atoms and those hydrogen atoms bonded to oxygen atoms are 1.5 times that of the atom to which they are attached.

Atomic Force Microscopy. General surface topographic imaging was performed using a Veeco Dimension V AFM, operated under the tapping mode (amplitude set point and scan rate were set at 340 mV and 0.8 Hz, respectively). Quantitative mechanical property mapping was carried out using a Bruker Dimension FastScan AFM, operated under the peak-force tapping mode (PeakForce QNM),[25] with which an amplitude set point of 250 mV was applied and the scan rate was set at 1 Hz. The type of tip used was TAP525A, designed for measuring the Young's moduli (E) in the range of 1 to 20 GPa; the performance of the probe was verified using a polystyrene standard ($E \approx 3$ GPa). The spatial distribution of E across the nanosheet surface was determined from the AFM load–displacement curves by applying the Derjaguin–Muller–Toporov model.[36] The Poisson's ratio of the sample was taken as 0.3.

Transmission Electron Microscopy. TEM was performed on a Philips (FEI) CM30 transmission electron microscope operating at 300 kV. Images and diffraction patterns were recorded on high dynamic range Ditabis image plates. The layered MnDMS material proved to be significantly beam sensitive, and even at the lowest recordable intensities any crystallinity was lost within less than 30 s. For this reason, all observations were carried out at approximately −180 °C using a liquid nitrogen cooled sample holder. The exfoliated MnDMS is sufficiently conductive that there are no visible specimen charging issues in the TEM.

Nanoindentation Studies. Nanoindentation was performed using an MTS Nanoindenter XP (Agilent) fitted with the dynamic Continuous Stiffness Measurement module. Defect-free and untwinned single crystals were first cold-mounted on the epoxy resin, followed by grinding and fine polishing with diamond suspensions to expose flat surfaces oriented in the {100}, {010}, and {001} planes. This procedure has been previously applied successfully for preparing single crystals of dense hybrid frameworks for nanoindentation studies.[32,37,38] Indentation measurements were carried out using a spherical diamond indenter tip ($R = 10\ \mu$m) to a maximum surface penetration depth of 1000 nm, under a prescribed strain rate of 0.05 s^{-1}. Indenter calibration was performed using a fused silica standard ($E = 72$ GPa). To determine the Young's moduli of the bulk crystal, the indentation load–displacement data were analyzed by applying the method of Oliver and Pharr.[39] The Poisson's ratio of the sample was taken as 0.3.

Acknowledgment. The authors would like to thank the European Research Council for funding (ERC Grant No. 227781). J.C.T. is especially grateful to Dr. Ian Armstrong and Dr. Drew Murray at Bruker UK Ltd. for the use of their Dimension FastScan AFM.

Supporting Information Available: Table S1 lists the crystallographic data of bulk MnDMS. Table S2 lists the data used for the critical shear stress analysis. Figures S1 and S2 show the Le Bail fit to the X-ray diffraction pattern of bulk MnDMS and the reconstituted nanosheets after ultrasonication, respectively. Figure S3 depicts the coordination environment around the Mn center. Figure S4 shows the TGA profile of bulk MnDMS. Figure S5 shows the TEM micrograph of the hexane-exfoliated nanosheets. Figure S6 depicts micromechanical delamination of hybrid layers *via* a spherical nanoindenter tip. X-ray crystallographic file (CIF) of the MnDMS structure. This material is available free of charge *via* the Internet at http://pubs.acs.org.

REFERENCES AND NOTES

1. Cheetham, A. K.; Rao, C. N. R.; Feller, R. K. Structural Diversity and Chemical Trends in Hybrid Inorganic-Organic Framework Materials. *Chem. Commun.* **2006**, 4780–4795.
2. Ajayan, P. M.; Schadler, L. S.; Braun, P. V.; Keblinski, P. *Nanocomposite Science and Technology*, 2nd ed.; Wiley-VCH Verlag GmbH & Co. KGaA, 2008.
3. Rao, C. N. R.; Cheetham, A. K.; Thirumurugan, A. Hybrid Inorganic-Organic Materials: A New Family in Condensed Matter Physics. *J. Phys. Condens. Matter.* **2008**, *20*, 083202.
4. Cheetham, A. K.; Rao, C. N. R. There's Room in the Middle. *Science* **2007**, *318*, 58–59.
5. Rosseinsky, M. J. Recent Developments in Metal-Organic Framework Chemistry: Design, Discovery, Permanent Porosity and Flexibility. *Microporous Mesoporous Mat.* **2004**, *73*, 15–30.
6. Kitagawa, S.; Kitaura, R.; Noro, S. Functional Porous Coordination Polymers. *Angew. Chem., Int. Ed.* **2004**, *43*, 2334–2375.
7. Férey, G. Hybrid Porous Solids: Past, Present, Future. *Chem. Soc. Rev.* **2008**, *37*, 191–214.
8. Lee, J.; Farha, O. K.; Roberts, J.; Scheidt, K. A.; Nguyen, S. T.; Hupp, J. T. Metal-Organic Framework Materials as Catalysts. *Chem. Soc. Rev.* **2009**, *38*, 1450–1459.
9. McKinlay, A. C.; Morris, R. E.; Horcajada, P.; Férey, G.; Gref, R.; Couvreur, P.; Serre, C. BioMOFs: Metal-Organic Frameworks for Biological and Medical Applications. *Angew. Chem., Int. Ed.* **2010**, *49*, 6260–6266.

10. Horike, S.; Shimomura, S.; Kitagawa, S. Soft Porous Crystals. *Nat. Chem.* **2009**, *1*, 695–704.
11. Shekhah, O.; Liu, J.; Fischer, R. A.; Woll, C. MOF Thin Films: Existing and Future Applications. *Chem. Soc. Rev.* **2011**, *40*, 1081–1106.
12. Zacher, D.; Shekhah, O.; Woll, C.; Fischer, R. A. Thin Films of Metal-Organic Frameworks. *Chem. Soc. Rev.* **2009**, *38*, 1418–1429.
13. Gascon, J.; Kapteijn, F. Metal-Organic Framework Membranes-High Potential, Bright Future? *Angew. Chem., Int. Ed.* **2010**, *49*, 1530–1532.
14. Mas-Balleste, R.; Gomez-Navarro, C.; Gomez-Herrero, J.; Zamora, F. 2D Materials: To Graphene and Beyond. *Nanoscale* **2011**, *3*, 20–30.
15. Sasaki, T.; Watanabe, M.; Hashizume, H.; Yamada, H.; Nakazawa, H. Macromolecule-Like Aspects for a Colloidal Suspension of an Exfoliated Titanate. Pairwise Association of Nanosheets and Dynamic Reassembling Process Initiated from It. *J. Am. Chem. Soc.* **1996**, *118*, 8329–8335.
16. Li, P. Z.; Maeda, Y.; Xu, Q. Top-Down Fabrication of Crystalline Metal-Organic Framework Nanosheets. *Chem. Commun.* **2011**, *47*, 8436–8438.
17. Amo-Ochoa, P.; Welte, L.; Gonzalez-Prieto, R.; Miguel, P. J. S.; Gomez-Garcia, C. J.; Mateo-Marti, E.; Delgado, S.; Gomez-Herrero, J.; Zamora, F. Single Layers of a Multifunctional Laminar Cu (I,II) Coordination Polymer. *Chem. Commun.* **2010**, *46*, 3262–3264.
18. Treacy, M. M. J.; Rice, S. B.; Jacobson, A. J.; Lewandowski, J. T. Electron-Microscopy Study of Delamination in Dispersions of the Perovskite-Related Layered Phases K-$[Ca_2Na_{n-3}Nb_nO_{3n+1}]$—Evidence for Single-Layer Formation. *Chem. Mater.* **1990**, *2*, 279–286.
19. Sasaki, T.; Watanabe, M.; Hashizume, H.; Yamada, H.; Nakazawa, H. Reassembling Process of Colloidal Single-Layers of an Exfoliated Titanate. *Chem. Commun.* **1996**, 229–230.
20. Golberg, D. Nanomaterials Exfoliating the Inorganics. *Nat. Nanotechnol.* **2011**, *6*, 200–201.
21. Osada, M.; Akatsuka, K.; Ebina, Y.; Funakubo, H.; Ono, K.; Takada, K.; Sasaki, T. Robust High-K Response in Molecularly Thin Perovskite Nanosheets. *ACS Nano* **2010**, *4*, 5225–5232.
22. Akatsuka, K.; Haga, M.; Ebina, Y.; Osada, M.; Fukuda, K.; Sasaki, T. Construction of Highly Ordered Lamellar Nanostructures through Langmuir-Blodgett Deposition of Molecularly Thin Titania Nanosheets Tens of Micrometers Wide and Their Excellent Dielectric Properties. *ACS Nano* **2009**, *3*, 1097–1106.
23. Coleman, J. N.; Lotya, M.; O'Neill, A.; Bergin, S. D.; King, P. J.; Khan, U.; Young, K.; Gaucher, A.; De, S.; Smith, R. J.; *et al.* Two-Dimensional Nanosheets Produced by Liquid Exfoliation of Layered Materials. *Science* **2011**, *331*, 568–571.
24. Fukuda, K.; Akatsuka, K.; Ebina, Y.; Ma, R.; Takada, K.; Nakai, I.; Sasaki, T. Exfoliated Nanosheet Crystallite of Cesium Tungstate with 2D Pyrochlore Structure: Synthesis, Characterization, and Photochromic Properties. *ACS Nano* **2008**, *2*, 1689–1695.
25. Pittenger, B.; Erina, N.; Su, C., Quantitative Mechanical Properties Mapping at the Nanoscale with Peakforce QNM. *Bruker Application Note #128* , **2011**.
26. Sweers, K.; van der Werf, K.; Bennink, M.; Subramaniam, V. Nanomechanical Properties of Alpha-Synuclein Amyloid Fibrils: A Comparative Study by Nanoindentation, Harmonic Force Microscopy, and Peakforce QNM. *Nanoscale Res. Lett.* **2011**, *6*.
27. *ASM Handbook*, Vol. 8: Mechanical Testing and Evaluation. ASM International: Materials Park, OH, 2000; p 77.
28. Tan, J. C.; Bennett, T. D.; Cheetham, A. K. Chemical Structure, Network Topology, and Porosity Effects on the Mechanical Properties of Zeolitic Imidazolate Frameworks. *Proc. Natl. Acad. Sci. U. S. A.* **2010**, *107*, 9938–9943.
29. Tan, J. C.; Cheetham, A. K. Mechanical Properties of Hybrid Inorganic-Organic Framework Materials: Establishing Fundamental Structure-Property Relationships. *Chem. Soc. Rev.* **2011**, *40*, 1059–1080.
30. Johnson, K. L. *Contact Mechanics*; Cambridge Univ. Press: Cambridge, 1985; pp 84—106.
31. Bei, H.; Lu, Z. P.; George, E. P. Theoretical Strength and the Onset of Plasticity in Bulk Metallic Glasses Investigated by Nanoindentation with a Spherical Indenter. *Phys. Rev. Lett.*. **2004**, *93*.
32. Tan, J. C.; Merrill, C. A.; Orton, J. B.; Cheetham, A. K. Anisotropic Mechanical Properties of Polymorphic Hybrid Inorganic-Organic Framework Materials with Different Dimensionalities. *Acta Mater.* **2009**, *57*, 3481–3496.
33. *Oxford Diffraction CrysAlisPro*; Oxford Diffraction Ltd.: Yarnton, Oxfordshire, England, 2010.
34. Sheldrick, G. M. A Short History of SHELX. *Acta Crystallogr., Sect. A* **2008**, *64*, 112–122.
35. Farrugia, L. J. *WinGX - A Windows Program for Crystal Structure Analysis*; University of Glasgow: Glasgow, UK, 1998.
36. Derjaguin, B. V.; Muller, V. M.; Toporov, Y. P. Effect of Contact Deformations on Adhesion of Particles. *J. Colloid Interface Sci.* **1975**, *53*, 314–326.
37. Tan, J. C.; Furman, J. D.; Cheetham, A. K. Relating Mechanical Properties and Chemical Bonding in an Inorganic-Organic Framework Material: A Single-Crystal Nanoindentation Study. *J. Am. Chem. Soc.* **2009**, *131*, 14252–14254.
38. Kosa, M.; Tan, J. C.; Merrill, C. A.; Krack, M.; Cheetham, A. K.; Parrinello, M. Probing the Mechanical Properties of Hybrid Inorganic—Organic Frameworks: A Computational and Experimental Study. *ChemPhysChem* **2010**, *11*, 2332–2336.
39. Oliver, W. C.; Pharr, G. M. Measurement of Hardness and Elastic Modulus by Instrumented Indentation: Advances in Understanding and Refinements to Methodology. *J. Mater. Res.* **2004**, *19*, 3–20.